ORIGINAL PAPER

Mechanism and future risk of slope instability induced by extreme rainfall event in Izu Oshima Island, Japan

Ikuo Towhata[1] · Satoshi Goto[2] · Shigeru Goto[3] · Takeshi Akima[4] · Junya Tanaka[4] · Taro Uchimura[5] · Gonghui Wang[6] · Hiroshi Yamaguchi[7] · Shogo Aoyama[8]

Abstract

A volcanic slope in Izu Oshima Island in Japan experienced a profound rain-induced disaster in October 2013. Since this slope had been stable for centuries except for minor failures, a special investigation was carried out on the cause. Because of its volcanic origin, the failed slope consisted of layers of ash, sand and lava. While the investigation concerned many disciplines, the present paper addresses one part of the geotechnical studies. The particular emphasis was put on the reason why some part of the slope "did not" fail because the post-disaster construction of infrastructures in the affected area relied on the future stability of the affected mountain slope. In line with this, another focus of the study was on the geohydrological feature of the underlying lava layer that possibly controlled the instability of the volcanic slope. It was concluded finally that the lava layer is pervious and allows drainage of infiltrated rainwater and that, only during extremely heavy rain, the subsurface lava topography triggered slope failure only in its "valley" parts. For 7 years after the disaster, the remaining parts of the slope have been stable as judged and many local infrastructures have been reconstructed.

Keywords Rainfall-induced disaster · Volcanic slope · Lava · Seepage · Restoration

✉ Ikuo Towhata
   towhata.ikuo.ikuo@gmail.com

1   Kanto Gakuin University, Yokohama, Japan

2   Yamanashi University, Kofu, Japan

3   Waseda University, Tokyo, Japan

4   Fudo Tetra Corporation, Tokyo, Japan

5   Saitama University, Saitama, Japan

6   DPRI, Kyoto University, Uji, Japan

7   Chuo Kaihatsu Corporation, Tokyo, Japan

8   University of Tokyo, Bunkyo City, Japan

1 Introduction

The volcanic Izu Oshima Island is located in the Pacific Ocean, 120 km south of Tokyo (Fig. 1), and is 9 km in EW and 15 km in NS directions. The central part of this island is occupied by active Mihara Yama Volcano of 758 m in height (Fig. 2). The nature in this island is preserved as a national park.

This island has been prone to two types of natural disasters caused by volcanic activities (Koyama and Hayakawa 1996) and typhoon-induced rainfalls. Figure 3 shows the history of eruption of Mihara Yama volcano. In the recent history, the events in 1684–1690 and 1777–1792 produced extensive lava flows that reached the sea and induced substantial damage. Another event in the fourteenth century (most probably in 1338) caused lava flow to the west of the mountain that reached the sea as well (Nakamura 1964; Disaster Prevention Board of Tokyo Metropolitan Government 1990). As a consequence of repeated volcanic activities, the mountain slopes in this island are composed of many layers of lava, loess and ash.

Volcanic mountain slopes are covered by the detritus. Because of high permeability and low shear strength of the material, in comparison with rocky slopes, volcanic slopes are more prone to catastrophic rainfall-induced failure as addressed by Ichinose (1960), Scott et al. (2001), Inokuchi (2003), Lavigne and Thouret (2003), Saucedo et al. (2008), Paguican et al. (2009), Matsushi et al. (2013) and De Vita et al. (2013) among many others. Heavy rains have repeatedly induced disasters on this island as well. In addition to a legendary large slope failure induced by heavy rain in 1740s, the typhoon No. 22 "Aida" in 1958 (or domestically known as Kanogawa Typhoon) brought 419 mm of precipitation and triggered a significant slope failure on the western slope of the Mihara Yama Volcano (Committee for Publication of Oshima's History 2000; Japan Meteorological Agency 1958). After the 1958 event, another and severer disaster occurred in 2013 with many slope failures under significant precipitation. A reconnaissance investigation on this disaster detected peculiar phenomena such as groundwater ejection from the slope surface and curiously stable slopes that survived the extreme precipitation. With these in mind, the authors conducted their investigation, aiming, firstly, to shed light on the possible

Fig. 1 Location of Izu Oshima Island

Fig. 2 Brief map of Izu Oshima Island with Mihara Yama Volcano at the center
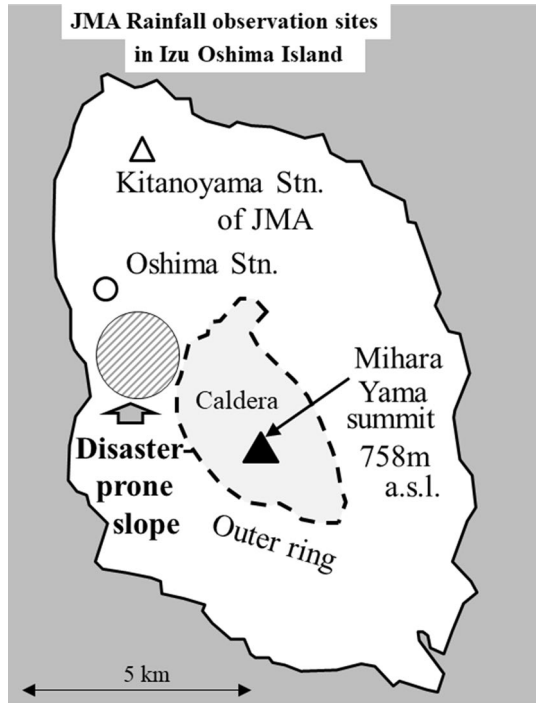
interaction between groundwater and slope stability and, secondly, to provide advices on risk of repeated slope disaster during the planned reconstruction of the affected community. Accordingly, the authors made efforts to understand why some parts of the slope failed and other parts did not in 2013.

2 Rainfall disaster during typhoon in 2013

The typhoon No. 26 "Wipha" in 2013 caused 824 mm of rainfall in Izu Oshima Island during 24 h from October 15 to 16. The hourly precipitation reached 122.5 mm/h from 2 to 4 AM on October 16. This event was the most devastating rainfall during the period from October 1939 to January 2019 (Fig. 4). As a consequence, slope failures were triggered at many places in the western side of Mihara Yama Volcano and the total area of slope failure was 319,000 m^2 with the failed soil volume = 175,000 m^3. A large amount of driftwood came down and aggravated the disaster. Consequently, 39 people were killed or missed, while 153 houses were affected (Tokyo Metropolitan Government 2014).

The first slope failure took place at around 2 AM and was followed by several more events until 4 AM. Those onset timings were assessed by referring to non-seismic ground shaking records in the island (National Research Institute for Earth Science and Disaster Resilience 2013; Ogiso and Yomogida 2015). The same slope was affected by the typhoon No. 22 in 1958, but the report by JMA (1958) indicates that the size of failure was smaller and its source was at lower elevation than in 2013.

Figure 5 demonstrates the view of the slope after the 2013 disaster. It is evident that many small earth flows merged to form a big one. Moreover, the initiation points were situated at the nick points of the volcanic slope where the slope is retrogressing toward the mountain. Noteworthy was that the nick points were situated slightly above the alignment of a motorway. Figure 6 exhibits one of the initiation points of the slope failure. Obviously, the depth of shear failure was shallow here. Shear failure developed above the interface between volcanic ash sand and less pervious loess soil underneath (Wang et al. 2019). Therefore, the slope disaster in 2013 was a part of the natural process in which mountain slope is eroded and disappears after a long time. After the initiation of instability, small failure mass merged with one another as travelling downward, eroded the slope surface and trees on the way (Fig. 7), increased the size and devastated the human community at the bottom (Fig. 8).

The base of the failed slope was made of volcanic materials that deposited mainly during the eruption in 1338 (Nakamura 1964; Disaster Prevention Board of Tokyo Metropolitan Government 1990). Since that year, this slope had not experienced sizeable failure for more than 650 years. Therefore, it may be said that the 2013 rainfall (Fig. 4)

Fig. 3 History of volcanic eruption of Mihara Yama Volcano (drawn after Disaster Prevention Board of Tokyo Metropolitan Government, 1990)
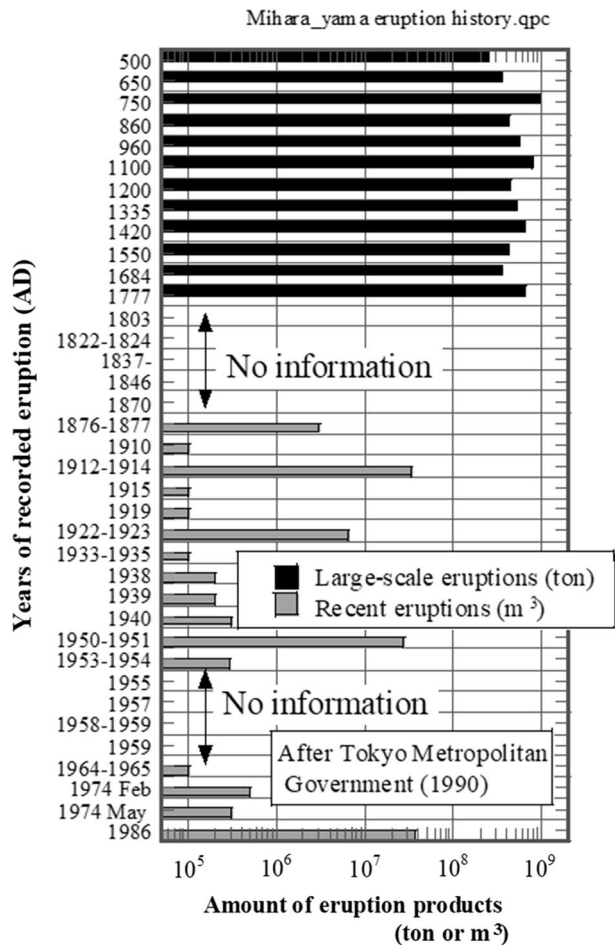
and associated slope failure were the extremely rare and severe events. One of the interesting findings in the disaster area is the existence of many piping holes (Fig. 9) through which a big amount of groundwater was ejected from the volcanic subsoil. There are different opinions about the creation of those piping holes; high groundwater pressure removed the surface material to trigger the slope failure, or falling-down of the surface material triggered water ejection. Rainfall-induced slope disaster in this island has been called "byaku" by local people. According to Tsuiki (1961), "byaku" means flow of debris and water triggered by ejection of groundwater (through piping holes).

3 Problems encountered during and after the disaster

During the post-disaster phase, an important issue was the reconstruction of the local community in the disaster-hit area. Both damaged infrastructures and safe life of people had to be reconstructed therein. In addition to the residential area, reconstruction of a motorway that connects the town and the top of the Mihara Yama Volcano was urgent for the benefit of tourism. Then, the question was whether or not the remaining parts of the slope would fall soon again. As shown in Fig. 5, approximately half of the slope area still remained at the original locations. In the past, many studies on slope disasters explained why slopes failed. In contrast, extremely few tried to understand why slopes did not. The present study explains why some parts of the slope did not fail in 2013. This task was not easy because of the limited time and budget.

Another issue was slope monitoring and early warning for the safety of local community. In case of rainfall-induced sediment disasters (slope failures and debris flows), warning of incipient heavy rainfall and evacuation order are inexpensive and very important. Accordingly, early warning based on rainfall intensity and duration has a long history of development and is widely practiced nowadays (Endo 1969; Onodera et al. 1974; Campbell 1975; Caine 1980; Terlien 1998; Nakai et al. 2007; Baum and Godt 2010; Brunetti et al. 2010; Osanai et al. 2010; Nolasco-Javier 2015; Piciullo et al. 2017; Segoni et al. 2018).

Noteworthy in early warning is that the rainfall criterion relies on the rainfall forecast and its measurement. Because the target area is vast, the warning cannot consider the local topography and soil properties. Apparently, it does not consider the effects of subsurface conditions such as shear strength of soil and underground hydrology whose importance

Fig. 4 History of severe rainfall records at Izu Oshima Station of Japanese Meteorological Agency
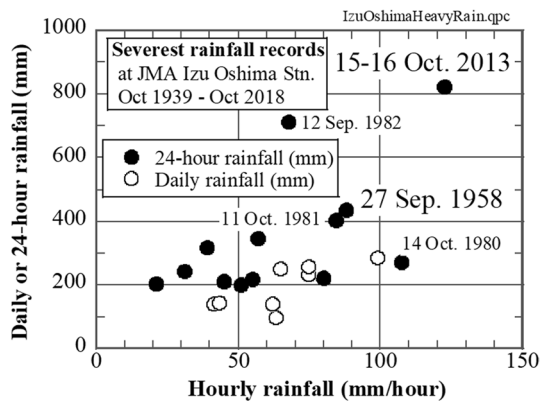
Fig. 5 View of failed slope on
the western side of Mihara Yama
Volcano

is inferred by the piping hole in Fig. 9. Moreover, all the factors such as rainfall intensity,
slope gradient and material properties change from place to place in the disaster area. Fig-
ure 10 illustrates two-times difference in rainfall intensity during the 2013 event at two
JMA stations (Oshima and Kitanoyama) whose locations are illustrated in Fig. 2. Hence, it
is difficult for the national government to conduct more reliable and site-specific forecast
and warning of slope disaster during heavy rain. Another problem in 2013 was the delayed
communication between the warning agency and the local government as well as affected
residents (Oshima Municipal Government 2016). These problems suggest need for differ-
ent and independent warning and evacuation activities that are conducted by local groups
in parallel to the national government's warning. It is further noteworthy in Fig. 10 that the
slope failure in 2013 occurred when the accumulated rainfall exceeded the total rainfall in
1958. This may suggest the immunity of slope that can resist failure until the maximum
past rainfall is exceeded.

4 Borehole investigation by the authors

In view of the aforementioned issues, the authors together with researchers of different
expertises conducted urgent studies in the island with a financial support from the national
government. The present paper addresses only the geotechnical aspects of their study.
Because the island is a national park under strict protection, all the works were carried out

Fig. 6 Shallow shear failure at
the initiation of slope instability

Fig. 7 Eroded surface in the middle of the mountain slope

Fig. 8 Destroyed human community at the base of the slope

Fig. 9 Piping holes at the head scarp of the failed slope

with permission by concerned public sectors and authorities. The major points in this study were material properties of the soil in the failed slope, geotechnical profile of the subsoil, roles played by groundwater and possibility of further disaster. It was aimed to thus contribute to the reconstruction of the local community.

Figure 11 illustrates the sites of the authors' study in which B, B' and C stand for the borehole sites, while those numbers 8–20 show the sites of borehole drilled by the Tokyo Metropolitan Government. All the holes were drilled after the disaster.

Figure 12 illustrates the situation of the points B and B' that are located below the top scarp of failure and beside a slope failure, respectively. B was on the failed slope, while B' was on a stable ground. By comparing these two sites, it was expected to find the reason why one part of the mountain slope was stable, while other part was not. Figure 13 compares the obtained subsurface profiles. The autobrecciated lava is a material that is formed by quick cooling and volume contraction. Within the range of drilling (down to 10 m depth), B' site has a thicker lava layer than B that is within the slope failure. Another point is that the unstable slope at B consists of interbedding different materials in which scoria and gravel appear more pervious than lava.

Photographs of drilled samples from B (failed slope) and B' (no failure) are compared in Fig. 14. Therein, the shallow parts are composed of fractured and highly pervious materials. At B in Fig. 14a, the material from GL−1 m to −3 m is called autobrecciated lava. Although it is named "lava," its appearance is similar to that of highly pervious gravel. Below 3.5 m, the profile in Fig. 14a is made of interbedding lava and gravelly materials. The top lava layer contains many fissures, but two more lava layers at lower elevations appear more continuous and less pervious. The profile at B' is characterized by a thicker lava layer from GL−5 m to −10 m; see Fig. 14b. Note, however, that this continuous lava layer has many cracks and appears to be pervious.
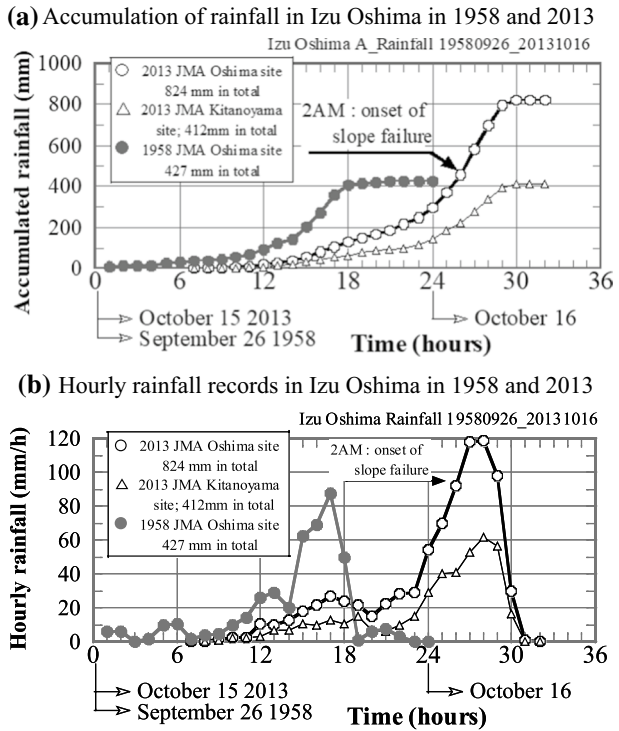
The borehole site C is located on a small mound within the damaged slope (Fig. 11). Herein, the original surface material had been removed by the soil flow and a lava layer was exposed at the surface (Fig. 15). The stratigraphy at C (Fig. 16) appears similar to that of the site B' (Fig. 13) where no failure happened. Note that ABL (autobrecciated lava) in Fig. 17 is a lava that was broken into small pieces during cooling. It is interesting that standard penetration resistance in ABL is quite variable, possibly depending on the extent of breakage and grain size.

The effect of the lava layer on underground water flow is an interesting issue. Some people believe that the lava layer is hardly pervious and the infiltrated rainwater is held within the surface layer, thereby reducing the slope stability. To shed light on this issue, a field permeability test was run on lava inside the borehole at C site. The obtained permeability was $k_1 = 1.07 \times 10^{-5}$ m/s for the depth of 6—7 m (thickness, $l_1, = 1$ m) and $k_2 = 3.20 \times 10^{-6}$ m/s for the depth of 7—8 m ($l_2 = 1$ m). The appearance of the collected lava specimens (Fig. 17) suggests that lava from 7 to 8 m depth is more continuous than upper and lower parts and that it is less pervious than others. Further, the lower part (8—9 m; $l_3 = 1$ m) appears as discrete as the upper part (6—7 m) and is reasonably assigned with higher permeability ($k_3 = 1.07 \times 10^{-5}$ m/s). Consequently, the seepage analysis in the later chapter will consider the lava layer to be pervious to a certain extent and employ a mean value of

$$k = \sum_i l_i / \sum_i \frac{l_i}{k_i} \tag{1}$$

for vertical water flow. In case of composition by three layers,

Fig. 10 Rainfall records at JMA Oshima and Kitanoyama Stations at 3 km distance from each other (for location of stations, see Fig. 2)

(a) Accumulation of rainfall in Izu Oshima in 1958 and 2013

(b) Hourly rainfall records in Izu Oshima in 1958 and 2013

$$k = \left(l_1 + l_2 + l_3\right) / \left(\frac{l_1}{k_1} + \frac{l_2}{k_2} + \frac{l_3}{k_3}\right) = 6.01 \times 10^{-6}\,\text{m/s} \tag{2}$$

No groundwater was encountered down to 20 m below the surface during the tests.

5 Borehole data over the entire width of the failed slope

Figure 5 shows that a substantial portion of the slope remained intact at the high elevation after the disaster (Fig. 18). Hence, the most important problem when community reconstruction was discussed after the disaster was the possibility of further slope failure in the coming years. To handle this problem, the authors borrowed more borehole data at the middle height of the slope from the Tokyo Metropolitan Government and interpreted them together with their own data at point C. The location of those boreholes is illustrated in Fig. 11, Nos. 8–20. After their interpretation, Fig. 19 is drawn. Prior to addressing its significance, the post-disaster situation at several borehole sites is picked up to illustrate that there were two different damage types as stated in the following sections.
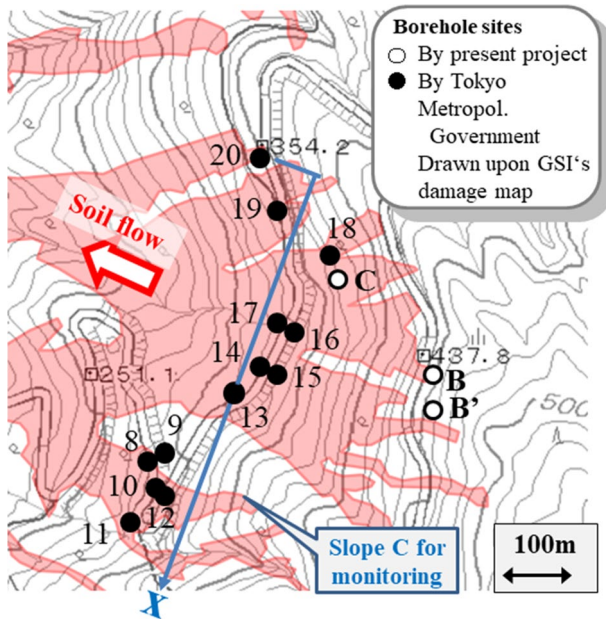
Fig. 11 Area of soil flow and borehole sites in the western slope of Mihara Yama Volcano (drawn on topographic map by Geological Survey Institute)

5.1 Site 8

At No. 8 site (Fig. 20), the surface soil and vegetation were lost by erosion but the road structure as well as a check dam in the top-left background remained intact. This implies that the slope did not fail by shear. This site is, therefore, called erosion-dominated.

5.2 Site 9

On the mountain side of the No. 9 site was a head scarp as shown in Fig. 21. Therefore, this site failed by shear failure mechanism. No piping hole was found here, and there is no idea about the effect of pore water pressure on shear failure.

5.3 Site 14

This site was affected by erosion. The person in Fig. 22 is standing on a mound that survived the disaster. Thus, no shear failure happened here.

5.4 Site 18

In Fig. 23, there are many piping holes in the head scarp behind this site. It is inferred therefore that effective stress here was reduced by water ejection and that shear failure triggered the slope disaster herein.

Fig. 12 Situation near boreholes B and B' during the subsurface investigation

(a) Borehole site B

(b) Borehole site B'

5.5 Site 20

The exact site of this borehole is located on an intact ground (Fig. 24a). However, there was a head scarp of failure accompanied by a piping hole within 1 m distance (Fig. 24b). Therefore, this site should be considered to have failed by shear mechanism.
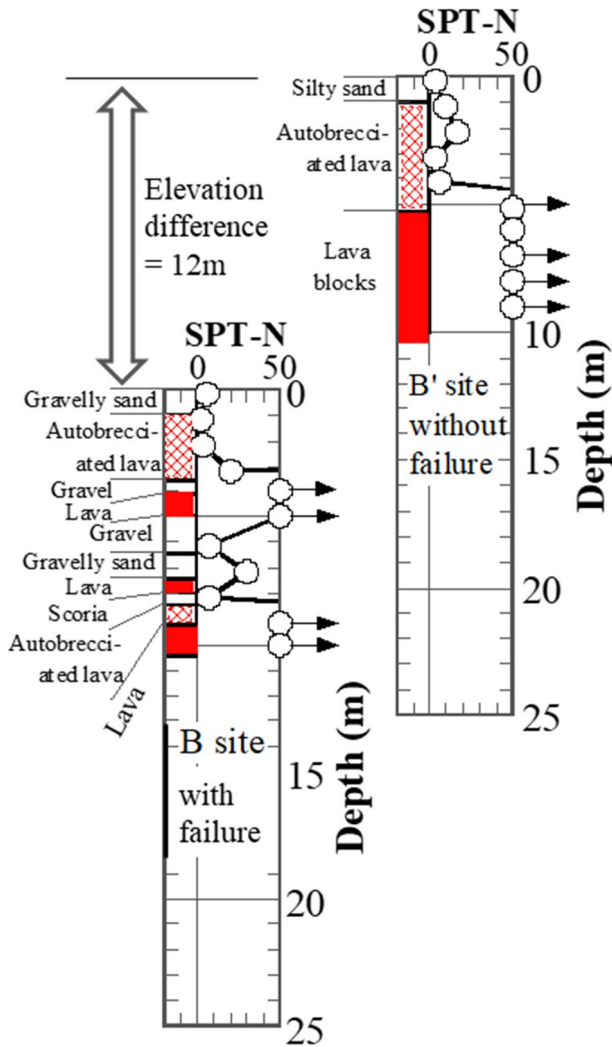
Fig. 13 Borehole profiles at sites with B and without B' slope failure

6 Reason why some part of the slope did not fail during extreme rainfall

The authors investigated the nature of the lava layer that is less permeable than other slope materials and probably played an important role in slope disaster during the heavy rain. Because the depth of the available borehole data was limited, the study had to be made only of the "first" shallowest lava layer group. The "first" group was defined arbitrarily as the shallow lava layers that are separated from a deeper lava by an interval of more than 2 m, e.g., see depth 4–5 m at B site in Fig. 14a. In what follows, the length of lava parts in the "first" group is denoted by l.

Fig. 14 Comparison of core samples obtained at sites with B and without B' slope failure

(a) B site within a failed slope

(b) B' site out of a failed slope
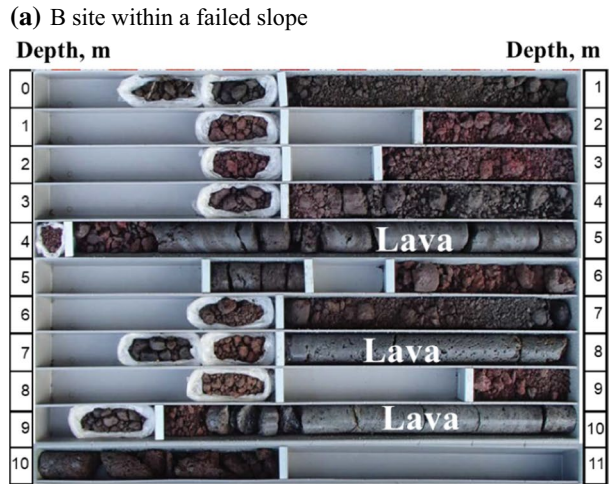
Fig. 15 Situation around borehole C

Fig. 16 Profile of borehole C
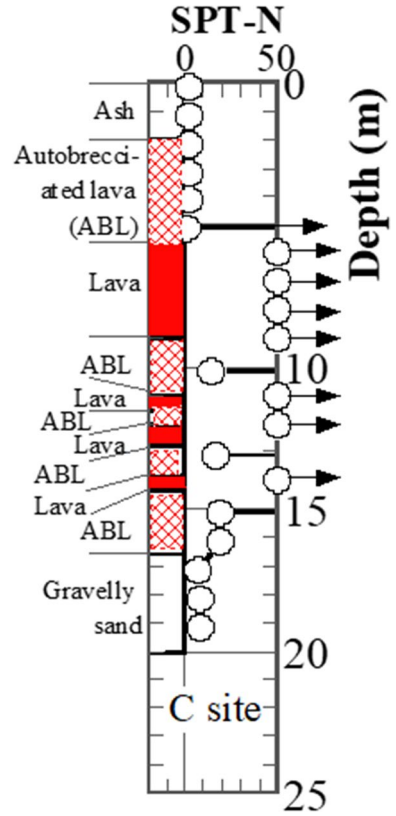
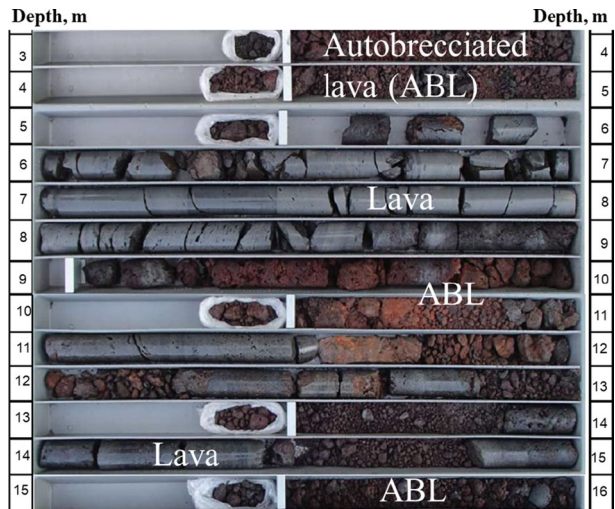**Fig. 17** Appearance of lava collected from depth 6–9 m of Site C

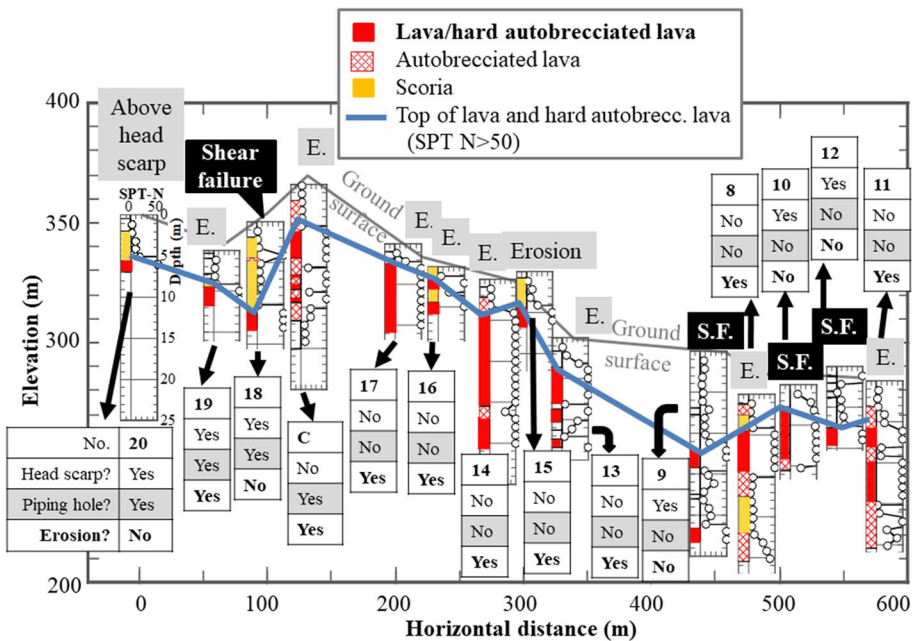**Fig. 18** Remaining parts of the disaster slope (view from the top)

Fig. 19 Cross section of failed slope obtained by interpretation of borehole data and type of damage; horizontal distance in this figure stands for the X coordinate in Fig. 11

Permeability of lava below surface soil was considered important for understanding the behavior of the entire affected slope during heavy rain. However, the limited research budget of the present study, as is also the case of most field practice, did not allow permeability tests to be conducted at many places. Therefore, the number of observed cracks per 1 m in respective lava layer is denoted by *m* and is used as a

Fig. 20 Post-disaster situation at borehole site No. 8

Fig. 21 Post-disaster situation at borehole site No. 9

Fig. 22 Post-disaster situation at borehole site No. 14

substitute for permeability. The greater the m number is, the more permeable is the lava; see Fig. 25 from the literature. Accordingly, the m number is used in place of permeability coefficient that was not measured in the field except at C site. By referring to Eq. 1, an alternative permeability parameter, k_{eq}, was defined by

$$k_{eq} = \sum_i l_i / \sum_i \frac{l_i}{m_i} \tag{3}$$

and the total thickness of lava parts in the first group, l_{eq}, was determined by

$$l_{eq} = \sum_i l_i \tag{4}$$

In principle, greater l_{eq} and smaller k_{eq} allow the first lava group to hold more water in soil above it. Hence, l_{eq}/k_{eq} is called "water-holding" index. The two indices are indicated in Fig. 26 in which borehole sites are classified into those with erosion only and those with shear failure. In general, the sites with erosion only have greater thickness of lava (l_{eq}) and higher water-holding capacity (l_{eq}/k_{eq}). Is it then reasonable to state that more rainwater was held in the surface soil at eroded sites and the slope "avoided" shear failure? This is not an acceptable idea because soil mechanics states that water saturation in a slope reduces the factor of safety against shear failure. One alternative idea is that the first lava layer group at eroded sites more efficiently reduced the upward flow of groundwater from deeper elevations and maintained surface stability than at sites of shear failure. However, the site 10 failed by shear in spite of similarly large index numbers, and hence, the above idea is not fully reliable. Thus, discussion should be made further from a different perspective.

Figure 19 is a summary of the interpretation of the post-disaster situation at borehole sites. At each site, three questions such as "Near head scarp?", "Having piping hole?" and "Affected by erosion failure?" were asked and answers are indicated in the same figure. By paying attention to the field situation (photographs), it was found that most sites were affected only by "erosion" at the surface and that "shear failure" of the subsoil happened at 4 sites. It was then attempted to relate these two types of damage with the borehole profile.

Fig. 23 Post-disaster situation at borehole site No. 18 (this photograph was taken during foggy hour of the day)
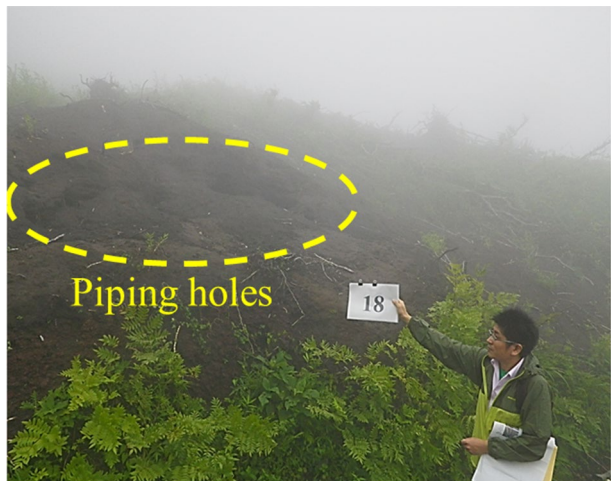
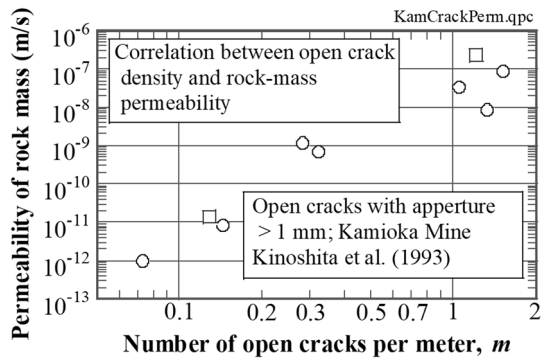**Fig. 24** Post-disaster situation at borehole site No. 20

(a) Exact site

(b) Nearby head scarp and piping hole

Fig. 25 Correlation between density of open cracks and permeability under similar overburden pressure (Kinoshita et al., 1993)

There is a layer of lava and autobrecciated lava in the slope. This lava is a product of the eruption in AD 1338 as stated previously. The autobrecciated lava is classified into two kinds in this figure according to the measured SPT-*N*. When the *N* value is greater than 50, the autobrecciated lava is considered to be stable and combined with the intact lava in illustration. Consequently, the top points of lava and hard autobrecciated lava in studied boreholes are connected in Fig. 19 to visualize the "subsurface topography."

Figure 19 also illustrates the type of damage which is either "shear failure" or "erosion" as discussed earlier. It is important that there is a reasonable correlation between the height of "subsurface topography" and the type of damage. Erosion damage occurred at the subsurface "ridge," while shear failure occurred in the buried "valley." Because the groundwater in the surface soil flows from "ridge" to "valley" during heavy rain, "shear failure" occurred in the "valley" parts: points 9, 10, 12 and 18, while point 8 is probably marginal. Conversely, the subsoil of the eroded parts was situated on "ridge" where groundwater flowed away. Hence, the "ridge" parts were intact until erosion during the disaster. Thus, there is a good reason why "ridge" parts of the slope did not fail during the heavy rain in 2013 and will remain stable during future heavy rains.

7 Simple analysis on slope stability and water flow in lava

Discussion in Fig. 19 was useful for practice but not quantitative. This chapter, in turn, addresses slope stability analysis with a special attention to water seepage from the surface toward the depth under gravity and an inverse flow from the depth upward through the first lava layer group.

7.1 Stability analysis

The shear failure occurred within the surface soil, and after field investigation, Wang et al. (2019) concluded that shear failure developed within the tephra layer which is situated

Fig. 26 Thickness and water-holding capacity of first lava layer group
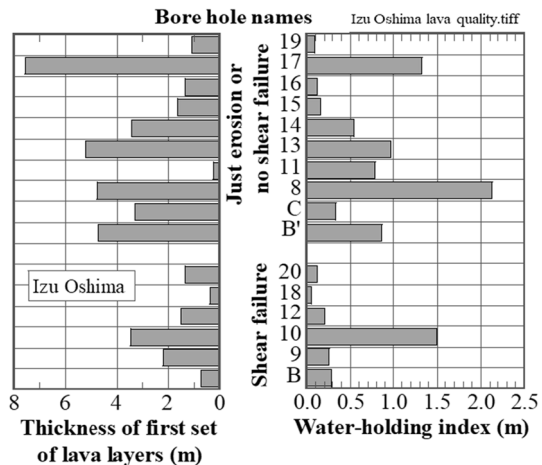
above less permeable loess (aeolian) soil. They collected disturbed samples of tephra from the affected slope and obtained the mean grain size (D_{50}) to be 0.17 mm and fines content $=21\%$. They also assessed the in situ dry density to be around 1.17 g/cm^3. Thereafter, ring shear tests on laboratory-reconstituted specimens (Wang et al. 2019) showed the friction angle, φ, of the failed surface soil to be around 38.5 degrees when materials were less compacted and hence weak (Fig. 27).

By using this value, a simple stability analysis was conducted on a one-dimensional slope model as shown in Fig. 28. In this model, the thickness of the unstable surface soil is denoted by H, the depth of groundwater above a hypothesized slip plane by h and the slope angle by $\theta = 30.5°$ based on the in situ topography near the head scarp. Furthermore, the unit weights of soil above and below the groundwater level were hypothesized without significant error as $\gamma_1 = 15.0$ kN/m^3 and $\gamma_2 = 19.1$ kN/m^3, respectively. Note that the common practice of borehole investigation in civil engineering projects hardly collects expensive undisturbed soil specimens and measures directly the unit weight. For stability analysis, the pore water pressure, u, at the slip plane (point B) was determined by making the total head at B equal to the head at the water surface (A). Since pore water pressure at A is zero,

$$u \text{ at } B = \gamma_w \times \text{(Elevation difference between A and B)} = \gamma_w h \cos^2\theta \qquad (5)$$

where γ_w stands for the unit weight of water. Then, the factor of safety, Fs, against shear failure is given by

$$\text{Fs} = \frac{\left[\{(H-h)\gamma_1 + h\gamma_2\}\cos\theta - u \times (1/\cos\theta)\right]\tan\varphi}{\{(H-h)\gamma_1 + h\gamma_2\}\sin\theta} = \frac{\tan\varphi}{\tan\theta}\left\{1 - \frac{\frac{h}{H}}{\left(1 - \frac{h}{H}\right)\frac{\gamma_1}{\gamma_w} + \frac{h}{H}\frac{\gamma_2}{\gamma_w}}\right\}$$

$$(6)$$

This calculation ignores the effects of partial saturation and matric suction on shear strength as well as those of heterogeneity of soil/rock properties. Those issues are considered herein too advanced for practical studies that have to be completed with limited time and budget.

Equation 6 is plotted in Fig. 29 by using $\varphi = 38.5°$ together with two other hypothetical values (30.5° and 40.5°). This figure indicates that the factor of safety becomes less than unity at $h/H = 0.4$ ($h = 40$ cm when $H =$ typically 1 m) when $\varphi = 38.5°$. The value of $H = 1$ m was chosen by referring to the soil thickness in the source area (Fig. 6). Even

Fig. 27 Stress paths obtained by constant-volume ring shear tests (Wang et al., 2019)
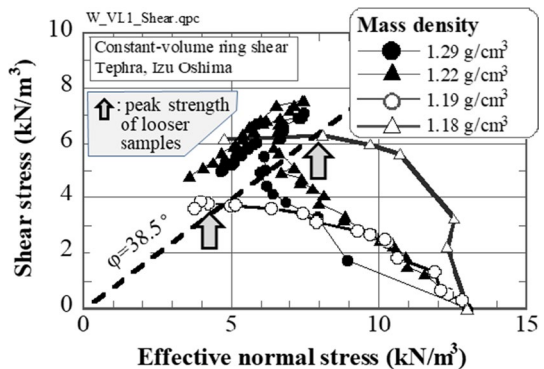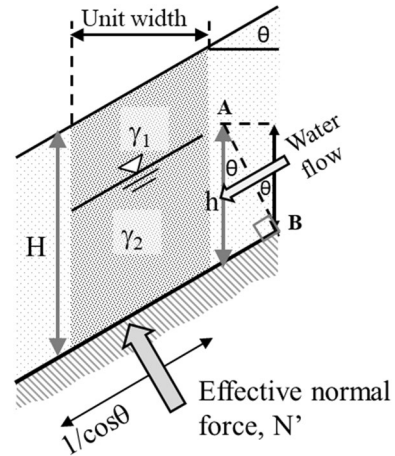
Fig. 28 Infinite slope model for stability analysis

for an overestimation of $\varphi = 40.5°$, $h/H = 0.55$ ($h = 55$ cm for $H = 1$ m) is sufficient to make the slope unstable. Such a shallow water depth is likely to occur frequently under the local rainfall environment (Fig. 4). Because the studied slope had been, on the contrary, stable for decades or for centuries in reality, further discussion is necessary.

7.2 Loss of water from surface soil into lava and deeper layers

Many studies on instability of volcanic slopes focused on the surface soil materials; see Fig. 28 as well as Pagano et al. (2014). In the present case, it seems necessary to shed more light on the role played by the underlying lava layer because the foregoing stability analysis on the surface soil underestimated the stability. Figure 30 presents a simple model of water infiltration from the ground surface through lava toward deep subsoil where water pressure is null. By using Darcy's law, the water flux is given by $v = ki = k(1 + h/l)$ where k stands for the permeability of the lava layer. When the groundwater surface is raised to reach the ground surface at C site (Fig. 16), $h = 6$ m and $l = 4$ m, while $k = 6.01 \times 10^{-6}$ m/s (Eq. 2) based on the aforementioned field permeability tests. Hence, $v = 1.50 \times 10^{-5}$ m/s or 54.1 mm/hour. Unless the rainfall intensity is continuously greater than 54 mm/hour or, 100 mm/hour if infiltration into subsoil is around 50% of the rainfall, the rainwater can be drained downward through the lava base and the surface soil cannot get fully saturated. Moreover, the void volume of the surface $h = 6$ m is given by $eh/(1 + e)$ where e stands for the void ratio. By hypothesizing $e = 0.7$, the void volume in top 6 m is equal to 2471 mm^3/ m^2. Hence, infiltration of, for example, 400 mm/hour should continue for 6 h for full saturation of soil. The hourly rainfall record in Fig. 10b suggests that such an extreme condition was hardly the case even during the two heavy rainfall events. Such an extreme rainfall event scarcely happens as illustrated in Fig. 31. This is the reason why the studied slope had avoided total failure for many decades in the past. To generate an unstable state of full saturation in the surface soil, more water supply is needed from elsewhere. One possible water source is given by the two-dimensional underground topography in Fig. 19 where groundwater flows from "ridge" to "valley."

The calculation above concerned only the intensity and duration of rainfall (400 mm/ hour and 6 h) but did not consider the detailed time history of rainfall. This is because more detailed calculation does not improve the accuracy of calculation when the true rainfall

Fig. 29 Effects of groundwater depth on slope stability in an infinite slope model
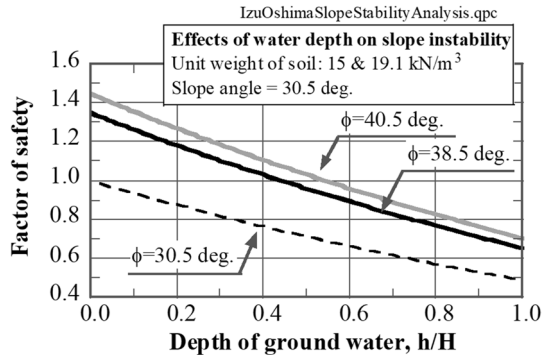

time history within the affected slope is unknown. Note further that the values of permeability were measured by field tests in dry season. Hence, the rock was not saturated with water and the obtained permeability corresponds to the unsaturated condition that may suit the real condition during heavy rain where groundwater level rises with time.

7.3 Possibility of upward flow of water through lava

Figure 9 suggests that water ejected from the underlying soil affected the initiation of slope instability. It was thus thought that high pore water pressure in subsoil played a chief role in the triggering mechanism of slope disaster. In this regard, this chapter examines the possibility of upward flow of groundwater through lava into surface soil. In extreme events, rainwater that infiltrates from the upper parts of the Mihara Yama

Fig. 30 Simple model for analysis on seepage flow into underlying lava layer
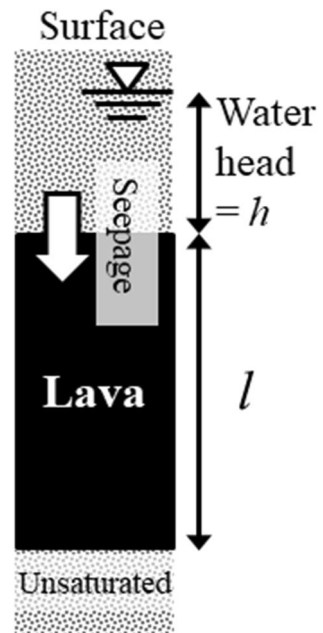
Volcano into the bottom of the slope may be able to seep through the lava layer and affect the surface stability. This situation is opposite from the previously discussed drainage down through the lava (Fig. 30). It can provide additional water and promote instability as stated in the previous section.

Figure 32 illustrates a simplified situation in which the base pervious layer is subject to high artesian water head of H_o that is maintained constant for a reasonably long time. Due to the upward seepage, the elevation of the groundwater surface, $h(t)$, increases with time. The upward hydraulic gradient, i, and the consequent water flow, v, are given respectively by

$$i = \frac{H_o - h}{h} \text{ and } v = \text{ki} = \frac{e}{1 + e} \times \frac{dh}{dt} \tag{7}$$

where e stands for the void ratio of lava layer. The right-hand side of the second equation stands for the void volume that the water flux of v fills during every unit time. By combining these two equations,

$$\frac{H_o - h}{h} = \frac{e}{(1 + e)k} \times \frac{dh}{dt}$$

$$1 - \frac{h}{H_o} = \frac{e}{(1 + e)kH_o} \times h\frac{dh}{dt} = \frac{eH_o}{(1 + e)k} \times \frac{h}{H_o}\frac{d}{dt}\left(\frac{h}{H_o}\right)$$

By introducing a time parameter, $t_* \equiv eH_o/\{(1 + e)k\}$

$$1 - \frac{h}{H_o} = \frac{t_*}{2}\frac{d}{dt}\left(\frac{h}{H_o}\right)^2$$

By integrating this,

$$t = \frac{t_*}{2} \int \frac{1}{1 - \frac{h}{H_o}}d\left(\frac{h}{H_o}\right)^2 = t_* \int \frac{\frac{h}{H_o}}{1 - \frac{h}{H_o}}d\left(\frac{h}{H_o}\right)$$

$$= t_* \int \left(-1 + \frac{1}{1 - \frac{h}{H_o}}\right)d\left(\frac{h}{H_o}\right) = -t_*\left\{\frac{h}{H_o} + \log_e\left(1 - \frac{h}{H_o}\right)\right\} + \text{const}$$

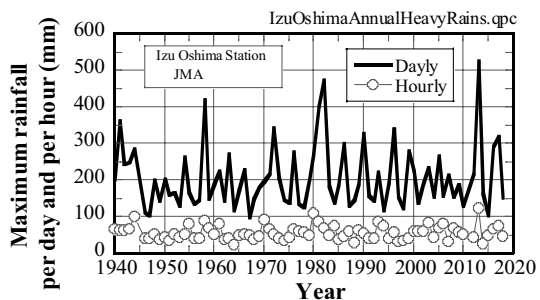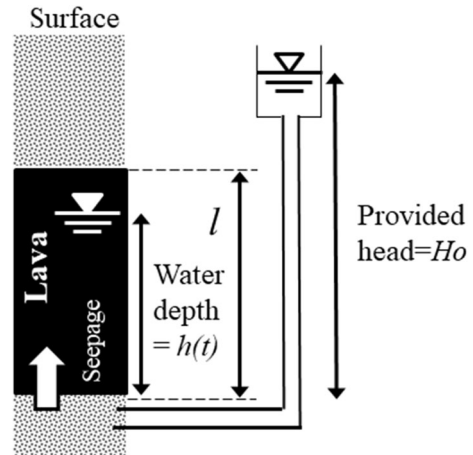**Fig. 31** Maximum daily and hourly rainfall records per year at JMA Oshima Station

Fig. 32 Model of groundwater flow upward through lava

By considering the initial condition of $h=0$ at $t=0$, the constant number is set equal to null. Hence,

$$\frac{t}{t_*} = -\left\{ \frac{h}{H_o} + \log_e\left(1 - \frac{h}{H_o}\right) \right\} \tag{8}$$

Figure 33 illustrates the relationship between t/t_* and h/H_o. It shows that h becomes equal to H_o (water table reaching the level of the external head) at the infinite time. In case of $e=0.7$, $H_o=20$ m and $k=6.01 \times 10^{-6}$ m/s, $t_*=1.37 \times 10^6$ s and the level of groundwater (h) reaches the top of lava ($h=l=4$ m in the previous example) at $t=31,700$ s $=8.8$ h only. After this time, groundwater from the bottom flows into the surface soil and affects slope stability therein. This simple analysis infers that a volcanic slope may be affected not only by the direct infiltration of rainwater from the surface but probably also by seepage of water that enters the underground regime from the mountain top and comes to the base of slope. This mechanism is certainly more critical in the "valley" subsurface topography where surface soil is thicker but lava layer is thinner (small l) than the "ridge." Figure 34 illustrates the effects of external water pressure (water head, H_o) on time needed for water flow to pass through the lava layer. As H_o increases, the required seepage time decreases drastically. It is unfortunate, however, that the present analysis remains conceptual and that it is extremely difficult to forecast H_o during the future heavy rain.

8 Situation in the slope after the disaster (2013–2018)

After the disaster, efforts were initiated to remove debris from the destroyed community and reconstruct infrastructures therein. In this stage, one of the most important issues was the risk of further slope failure and Fig. 19 is the authors' suggestion to the local community, further disaster being unlikely on the remaining "ridge" subsurface topography. To ascertain the safety of reconstruction activities, the authors installed an inexpensive early warning system in which tilting angle of sensors was monitored and interpreted. It has been a practice that a warning message is issued if the rate of tilting exceeds 0.1 degree/h. For

Fig. 33 Rising water level in lava layer caused by high pore water pressure underneath
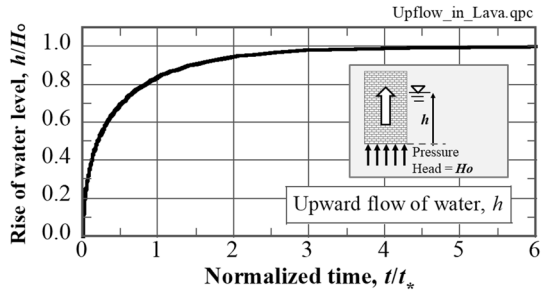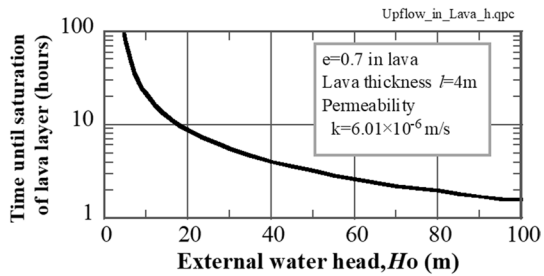

Fig. 34 Example calculation on time at which water level reaches the top of lava layer

details, refer to Uchimura et al. (2015) and Towhata et al. (2015). It is believed that this site-specific warning is supplementary to the rainfall-threshold principle of early warning as discussed previously.

Figure 35 illustrates one of the monitored sites that appeared more likely to fail soon than others, which is namely the slope C at the bottom of Fig. 11. The tilting angle of the device was recorded in 2014 as shown in Fig. 36a. Herein, the tilting angle made noticeable increase twice, in May and in October. The event in May occurred without rain, and it was supposed that the device tilted due to such a local disturbance as animal action (Fig. 36b). Therefore, no risk of slope failure was considered. In contrast, the October event occurred after typhoon No. 18 "Phanfone" brought precipitation of 162.5 mm on October 5 and 93.0 mm on 6 at JMA Oshima Station (Fig. 36c); effects of antecedent rainfall on slope instability. Therefore, attention was paid to the rate of tilting which is the key precursor data for safety judgment. Although an alert was prepared when the rate exceeded the warning criterion of 0.1 deg/h for a short while (Fig. 36d), this critical situation did not last for a long time and no slope failure happened.

The studied slope has been stable to date. On September 11, 2018, almost 5 years after the disaster, the first author visited the site and inspected the situation. It was found that the affected slope had been recovered by greening and that no serious slope failure had happened since 2013 (Fig. 37). The slope C of monitoring in Fig. 35 had maintained its stability for 6 years after the disaster (Fig. 38). Thus, the implication of Fig. 19 was confirmed to be reasonable.

Fig. 35 Installation of tiltometers for early warning of slope failure (photograph taken in 2014 by looking up from the slope bottom)
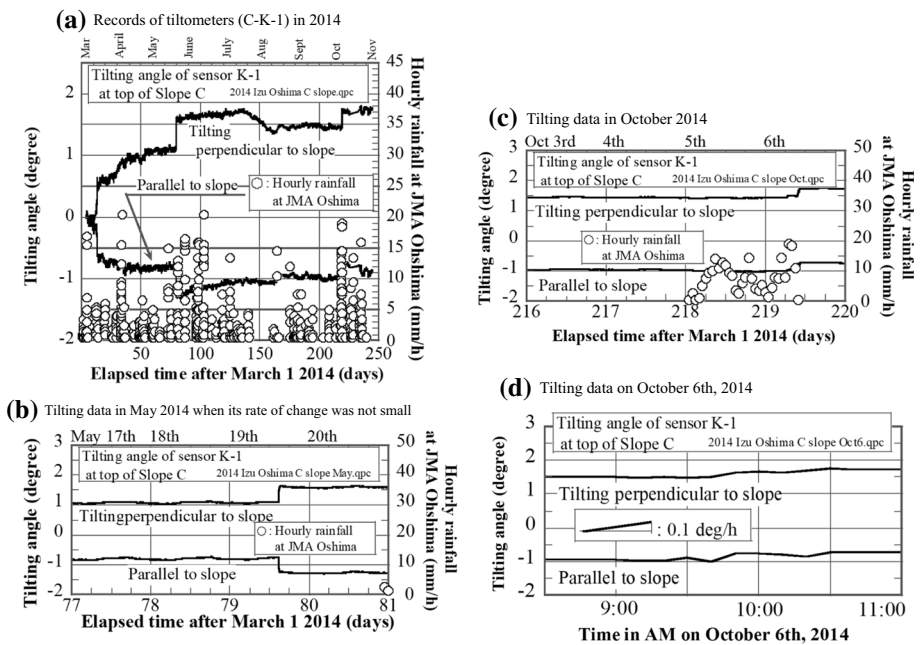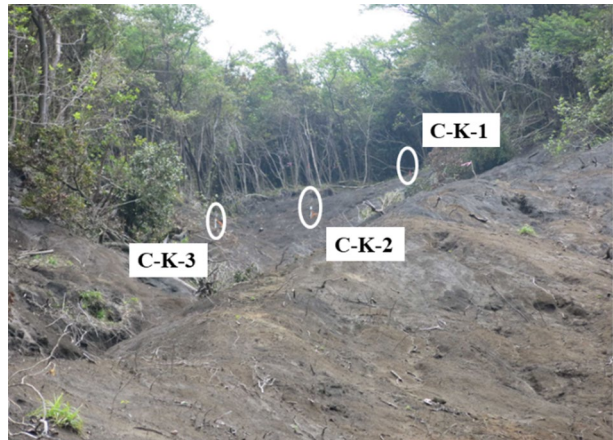

Fig. 36 Monitored records in 2014 at the top of the slope in Fig. 35

9 Conclusion

The present paper addresses the rainfall-induced slope disaster in Izu Oshima Island, Japan, in October 2013 when an extremely heavy precipitation came to the island. Because the failure occurred in a volcanic slope that had been stable for many centuries and also a practical concern was made of the possible repetition of similar disaster, efforts were made to understand the difference between failed slopes and slopes that remained stable during the heavy rain. The major conclusions drawn from this study are described in what follows.

Fig. 37 Intact situation of the failed slope on September 11, 2018 (same site as in Fig. 20)

Fig. 38 Intact situation of the monitored slope on September 11, 2018

(1) The extent of heavy rain changes from place to place together with the topography of mountains and local geology or soil conditions. Therefore, a regional warning of rainfall-induced slope disaster is not sufficient and there is a need to develop more site-specific warning method.

(2) Field reconnaissance found many piping holes in the source area of induced slope failures. The triggered slope instability was shallow at the initiation but increased its size by eroding surface materials as moving downward.

(3) The induced slope damages were classified into that of shear failure and that of erosion. The eroded slopes did not have sliding movement. The difference between two groups was caused by the subsurface topography of lava layer.

(4) By using this finding, the remaining part of the mountain slope was judged to be stable and the reconstruction of the affected community was recommended. To date (August 2020), no slope failure has happened there.

(5) The lava layer is pervious to a certain extent contrary to the general perception. Because of this permeability, infiltrated rainwater is drained easily into deep parts of the slope and does not remain in the surface soil. This is probably the main reason why this volcanic slope had not failed significantly during heavy rain events in the past.

(6) The intensity of rainfall in 2013 and possibly of the one in 1958 exceeded the drainage capacity of the underlying lava layer, and slope failure was triggered (with limited scale in 1958).

(7) Because the entire island is made of a pervious volcanic material, an attempt was made to understand the effect of artesian water pressure under the lava layer. It was found that the artesian water, if its pressure is high, can seep upward through the lava and affect the surface soil stability within a realistic period of time. It is, however, very difficult to forecast the artesian water pressure during the coming heavy rain.

Compliance with ethical standards

Conflict of interest The authors declare that they have no conflict of interest.

References

Baum RL, Godt W (2010) Early warning of rainfall-induced shallow landslides and debris flows in the USA. Landslides 7(3):259–272

Brunetti MT, Peruccacci S, Rossi M, Luciani S, Valigi D, Guzzetti F (2010) Rainfall thresholds for the possible occurrence of landslides in Italy. Nat Haz Earth Syst Sci 10(3):447–458

Caine N (1980) The rainfall intensity: duration control of shallow landslides and debris flows. Geografiska annaler: series A, physical geography. Svenska Sallskapet för Antropologi och Geografi (Swedish Soc Anthropol Geogr) 62(1/2):23–27

Campbell RH (1975) Soil slips, debris flows, and rainstorms in the Santa Monica mountains and vicinity geological survey professional paper. US Geological Survey Professional Paper, Southern California, p 851

Committee for Publication of Oshima's History (2000) General Summary of Oshima History, p.765 (in Japanese).

De Vita P, Napolitano E, Godt JW, Baum RL (2013) Deterministic estimation of hydrological thresholds for shallow landslide initiation and slope stability models: case study from the Somma-Vesuvius area of southern Italy. Landslides 10(6):713–728

Disaster Prevention Board of Tokyo Metropolitan Government (1990) Characteristics on volcanic activities in Izu Archipelago, p.40 (in Japanese).

Endo T (1969) Probable distribution of the amount of rainfall causing landslides, Annual Report 1968, Hokkaido Branch, Government Forest Experiment Station, 122-136 (in Japanese).

Ichinose Y (1960) On landslides at Tara Volcano, northern Kyushu. Geogr Rev Japan 33(10):515–528

Inokuchi T (2003) General report of research on landslide disaster in quaternary volcanic areas. J Japan Landslide Soc 40(1):1–9 **(in Japanese)**

Japan Meteorological Agency (1958) Kanogawa typhoon. Technical Report, 37, p.140 (in Japanese).

Kinoshita N, Abe T, Takemura T, Yokomoto S (1993) Investigation of hydraulic properties in rock mass around tunnels using injection test. 25th Rock Mechanics Symposium, JSCE: 481–485 (in Japanese).

Koyama M, Hayakawa Y (1996) Syn- and post-caldera eruptive history of Izu Oshima volcano based on tephra and loess stratigraphy. J Geogr Tokyo Geogr Soc 105(2):133–162 **(in Japanese)**

Lavigne F, Thouret JC (2003) Sediment transportation and deposition by rain-triggered lahars at Merapi volcano, Central Java. Indonesia Geomor 49(1–2):45–69

Matsushi Y, Saito H, Fukuoka H, Furuya G (2013) Landslides of tephra deposits on hillslopes of the Aso Caldera wall and volcanic central cones by the North-Kyushu heavy rainfall at July 2012. Annu Disaster Prev Res Instit Kyoto Univ 56B:237–241 **(in Japanese)**

Nakai S, Kaibori M, Sasaki Y, Moriwaki T (2007) Applicability of a new rainfall index R′ for recent cases and proposal of the method for warning against sediment-related disaster. J Japan Soc Eros Control Eng 60(1):37–42

Nakamura K (1964) Volcano-Stratigraphic Study of Oshima Volcano, Izu. Bull Earthq Res Instit Univ Tokyo 42(4):649–728 **(in Japanese)**

National Research Institute for Earth Science and Disaster Resilience (2013) Records of ground shaking induced by slope disaster in Izu Oshima Island. Report, https://www.bosai.go.jp/saigai/2013/img/20131021_02.pdf retrieved on January 19, 2019 (in Japanese).

Nolasco-Javier D, Kumar L, Tengonciang AMP (2015) Rapid appraisal of rainfall threshold and selected landslides in Baguio, Philippines. Nat Haz 78(3):1587–1607

Ogiso M, Yomogida K (2015) Estimation of locations and migration of debris flows on Izu-Oshima Island, Japan, on 16 October 2013 by the distribution of high frequency seismic amplitudes. J Volcanol Geoth Res 298:15–26

Onodera T, Yoshinaka R, Kazama H (1974) Slope failures caused by heavy rainfall in Japan. J Japan Soc Eng Geol 15(4):191–200

Osanai N, Shimizu T, Kuramoto K, Kojima S, Noro T (2010) Japanese early-warning for debris flows and slope failure using rainfall indices with radial basis function network. Landslides 7(3):325–338

Oshima Municipal Government (2016) External committee report on sediment disaster in Izu Oshima Island in 2013, https://www.town.oshima.tokyo.jp/uploaded/life/1421_1711_misc.pdf retrieved on Jan. 17, 2019 (in Japanese).

Pagano L, Reder A, Rianna G (2014) Experiments to investigate the hydrological behaviour of volcanic covers, the third Italian workshop on landslides. Proced Earth Planet Sci 9:14–22

Paguican EMR, Lagmay AMF, Rodolfo KS, Rodolfo RS, Tengonciang AMP, Lapus MR, Baliatan EG, Obillem EC (2009) Extreme rainfall-induced lahars and dike breaching, 30 November 2006, Mayon Volcano, Philippines. Bull Volcanol 71(8):845–857

Piciullo L, Gariano SL, Melillo M, Brunetti MT, Peruccacci S, Guzzetti F, Calvello M (2017) Definition and performance of a threshold-based regional early warning model for rainfall-induced landslides. Landslides 14(3):995–1008

Saucedo R, Macías JL, Sarocchi D, Bursik M, Rupp B (2008) The rain-triggered Atenquique volcaniclastic debris flow of October 16, 1955 at Nevado de Colima Volcano, Mexico. J Volcanol Geoth Res 173(1–2):69–83

Scott KM, Macías JL, Naranjo JA, Rodriguez S, McGeehin JP (2001) Catastrophic debris flows transformed from landslides in volcanic terrains: mobility, hazard assessment and mitigation strategies. USGS Professional Paper, No. 1630

Segoni S, Piciullo L, Gariano SL (2018) A review of the recent literature on rainfall thresholds for landslide occurrence. Landslides 15:1483–1501

Terlien MTJ (1998) The determination of statistical and deterministic hydrological landslide-triggering thresholds. Environ Geol 35(2–3):124–130

Tokyo Metropolitan Government (2014) Report of Committee on disaster mitigation plan after slope disaster in 2013 **(in Japanese)**.

Towhata I, Uchimura T, Seko I, Wang L. (2015) Monitoring of unstable slopes by MEMS tilting sensors and its application to early warning. International Symposium on Geohazards and Geomechanics, Warwick, IOP Conference Series: Earth and Environmental Science.

Tsuiki T (1961) Study on history of Izu Oshima. Special committee for publication **(in Japanese)**

Uchimura T, Towhata I, Wang L, Nishie S, Yamaguchi H, Seko S, Qiao JP (2015) Precaution and early warning of surface failure of slopes by using tilt sensors. Soils Found 55(5):1086–1099

Wang G, Jiang Y, Chang C, Doi I, Kamai T (2019) Volcaniclastic debris avalanche on Motomachi area of Izu-Oshima, Japan, triggered by severe storm: phenomenon and mechanisms. Eng Geol 251:24–36